Available online at www.sciencedirect.com
SCIENCE DIRECT
Journal of Power Sources 158 (2006) 689–704
JOURNAL OF POWER SOURCES
www.elsevier.com/locate/jpowsour

Thermal runaway in VRLAB—Phenomena, reaction mechanisms and monitoring

D. Pavlov *, B. Monahov, A. Kirchev, D. Valkovska

Institute of Electrochemistry and Energy Systems (former CLEPS), 1113 Sofia, Bulgaria

Received 14 April 2005; received in revised form 8 September 2005; accepted 13 September 2005
Available online 8 November 2005

Abstract

During operation of the oxygen cycle water decomposes forming O_2 at the lead dioxide electrode, while at the lead electrode O_2 is reduced forming water. The mechanism of these processes is related with thermal phenomena as a result of which heat is released. When the cell temperature increases substantially the battery can be damaged. This phenomenon is often called thermal runaway (TRA). The present work investigates the changes in positive and negative plate potentials, temperature, current, and gassing rate during thermal runaway. It is established that during TRA maximums in the transient curves of positive plate potential, current, and finally cell temperature appear. These maximums mark four periods in the development of the TRA phenomenon. The processes that take place during each of these periods are elucidated. On ground of the experimental results a model of the electrochemical and chemical reactions that take place in the system is proposed. The thermal effects of these reactions lead to increase of the cell temperature. Water decomposition at the positive plate and water formation at the negative one cause changes in the concentration of H_2SO_4 at the plate interfaces. When the applied cell voltage is high the increase of the temperature and the changes in H_2SO_4 concentration lead to changes in the structure and phase composition of the electrodes interfaces. This results in changes of the type of the reactions that proceed at the two interfaces. Exothermic chemical reactions take place at the negative plate. Due to the increased temperature and H_2SO_4 concentration the positive plate partially passivates and the current goes through maximum and starts to decrease. The changes in Pb/solution interface and the decreased O_2 flow lead to a maximum in the cell temperature. Problems appear when the value of this maximum becomes higher than the temperature limit below which the battery operates normally.

On ground of this model of the thermal phenomena during OxCy operation the limits in the cell current and voltage as well as the thickness and type of the separator for which appearance of TRA does not cause battery damage are determined.

Keywords: Thermal runaway; Valve regulated lead acid battery; Oxygen cycle; Reactions involved in oxygen cycle; Oxygen reduction on lead electrode

1. Introduction

Valve regulated lead acid batteries (VRLAB) comprise two electrochemical systems: (a) current generating and accumulating system ($Pb/PbSO_4/H_2SO_4/PbSO_4/PbO_2$) and (b) oxygen cycle ($H_2O/O_2/H_2O{\cdot}H_2SO_4/O_2/H_2O$). The role of the second electrochemical system is to reduce the water loss during charging of the first one and to make the battery practically maintenance free [1–3]. For the operation of the oxygen cycle (OxCy), certain amount of electrical energy has to be introduced into the cell. As a result, oxygen is formed at the positive plate and is then reduced fully or partially at the negative plate. The latter process is associated with heat evolution within the battery. The heat is generated due to: (a) exothermic chemical reactions proceeding at the negative plate and (b) Joule effects. The evolved heat causes the cell temperature to increase. In some cases the temperature rises to a certain value and levels off, but in others the temperature increase becomes uncontrollable and may lead to battery failure. These phenomena are called, respectively, temperature rise (TR) and thermal runaway (TRA), and are illustrated in Fig. 1.

The thermal phenomena in VRLAB are widely discussed in the literature. Giess [4] and Haering and Giess [5] used a thermal video imaging system to investigate the thermal processes. Pesaran and co-workers investigated the thermal problems arising in EV and HEV batteries using coupled calorimetric-electrochemical device and proposed a battery thermal management system [6–8]. Culpin examined the influence of the

* Corresponding author. Tel.: +359 2 9710083; fax: +359 2 731552.
E-mail address: dpavlov@labatscience.com (D. Pavlov).

0378-7753/$ – see front matter © 2005 Elsevier B.V. All rights reserved.
doi:10.1016/j.jpowsour.2005.09.022

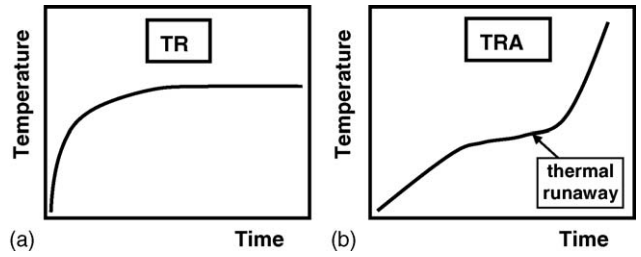

Fig. 1. Temperature changes in a VRLA cell during operation of the oxygen cycle: (a) temperature rise and (b) thermal runaway.

separator structure on thermal runaway [9]. Wagner discussed the influence of thermal phenomena on the performance of VRLAB [10]. Li et al. studied the influence of temperature and state of charge (SOC) on the rate of recombination of H_2O during OxCy [11]. In our previous work, we determined the energy balance of the oxygen cycle [12] and elucidated the mechanisms of the reactions of oxygen evolution at the positive plate [13,14] and oxygen reduction at the negative plate [15]. Robinson and Taras-con found that when VRLABs operate at temperatures above 60 °C hydrogen sulfide and sulfur dioxide are formed within the batteries [16]. Several experimental works on TRA phenomena were performed [17–21] and management systems for control of the thermal phenomenon were proposed [20–22].

The aims of the present work are:

(a) to determine the thermal phenomena involved in the OxCy and the processes which cause TRA in VRLAB;
(b) to elucidate the stages in the development of these phenomena and to identify the processes that take place during each stage;
(c) to determine the main parameters that control the intensity of the TRA phenomenon;
(d) to propose methods for limiting the effect of TRA to acceptable levels.

2. Experimental

2.1. Experimental procedure

All experiments were performed with fully charged cells. Therefore, only the reactions of the oxygen cycle proceeded during polarization. The experiments were conducted at the following voltages: 2.65 V, 2.60 V, 2.55 V, 2.50 V, 2.45 V, and 2.40 V.

In order to identify the phenomena that take place during thermal runaway (TRA) we measured the following parameters: cell voltage (U), positive and negative plate potentials versus Ag/Ag_2SO_4 reference electrode (φ^+ and φ^-), cell temperature (T), rate of gas going out of the cell, when the efficiency of the oxygen cycle was lower than 100% (dV_{out}/dt), and current flowing through the cell (i). The cell current was allowed to increase up to 10 A, which was the upper limit of the experimental set-up.

In order to elucidate the influence of the TRA effect on the active masses after finishing every experiment we determined the phase composition and structure of the positive and negative active masses as well as their crystal morphology.

2.2. Model cells and experimental set-up

Model cells (2 V/4 Ah) were assembled in transparent polymer cases. The grids of the positive and negative plates were cast from Pb–2% Sn alloy. The plates were formed and dried (the

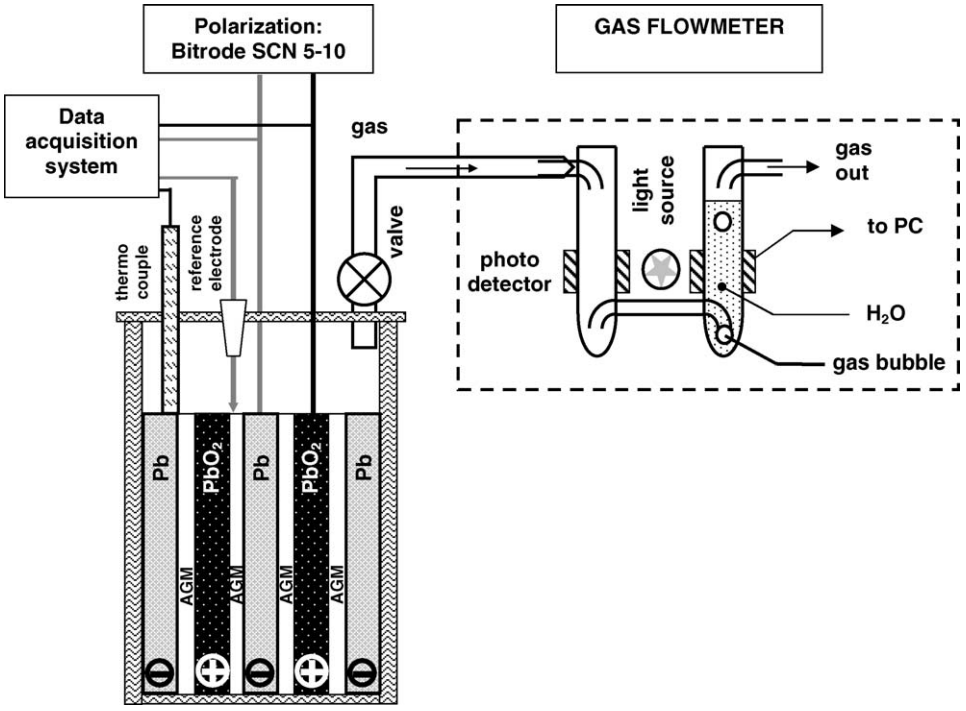

Fig. 2. Scheme of the experimental set-up.

negative ones in nitrogen atmosphere), weighed and then assembled dry charged in the cell. Two types of separators were used: absorptive glass mat (AGM) (Hollingsworth & Vose) and modified absorptive glass mat (MAGM) [23]. Each cell was fitted with a valve, an Ag/Ag_2SO_4 reference electrode [24] and a thermocouple mounted inside the cell. The gas leaving the cell through the valve was forced to pass through a flow meter (gassing rate monitoring system designed in this laboratory) [25]. A diagrammatical picture of the experimental set-up is presented in Fig. 2.

Bitrode SCN 10-5 test modules were used to maintain constant current or constant voltage in the model cells. The data from the measuring instruments were collected using a 16-channel computerized data acquisition system. The above six parameters were registered continuously during the experiment.

3. Experimental results

3.1. Thermal phenomena in VRLA cells

The experimental data for the cell current i, positive and negative electrode potentials φ^+ and φ^-, cell temperature T, and gassing rate dV_{out}/dt, as a function of time at two constant potentials ($U = 2.45$ V and 2.40 V) are plotted in Figs. 3 and 4, respectively. The cell is assembled with one sheet (2.2 mm) of AGM separator wrapping the positive plate. The results show that when the cell is polarized at 2.45 V, after 18 min the current starts to increase rapidly and reaches 9 A in less than 45 min (Fig. 3a). The cell temperature increases reaching 57 °C at the end of polarization (Fig. 3c).

After 1 h of polarization at 2.40 V, certain conditions are created in the cell at which maximums in φ^+, i, and T appear one after the other during 5 h of polarization. These maximums in the monitored parameters mark the different stages in the development of the TRA. Four periods can be distinguished: period A—from the beginning of the experiment to φ^+_{max}; period B—between φ^+_{max} and i_{max}; period C—between i_{max} and T_{max}; and period D—from T_{max} until i and T reach stationary values.

3.2. Processes taking place during the four periods in the development of the TRA phenomenon

The different stages in the TRA phenomenon are illustrated in Fig. 5 through the dependences of the positive and negative plate potentials (φ^+ and φ^-), and the gassing rate (dV_{out}/dt) on current (i) and temperature (T) for $U = 2.40$ V. The dashed lines mark the margins of the four periods. As all experiments are carried out at constant cell voltage, when the potential of the positive electrode increases the potential of the negative one must decrease and vice versa. Hence, the processes that take place at the two electrodes are interrelated. During each stage, one of the electrodes is independent and determines the potential of the other electrode. We will call the former electrode *master-electrode* and the latter one *slave-electrode*. Let us assume that the master-electrode is the one whose potential decreases (the results below will confirm this conjecture). Now let us see what happens during each of the four periods of the TRA phenomenon.

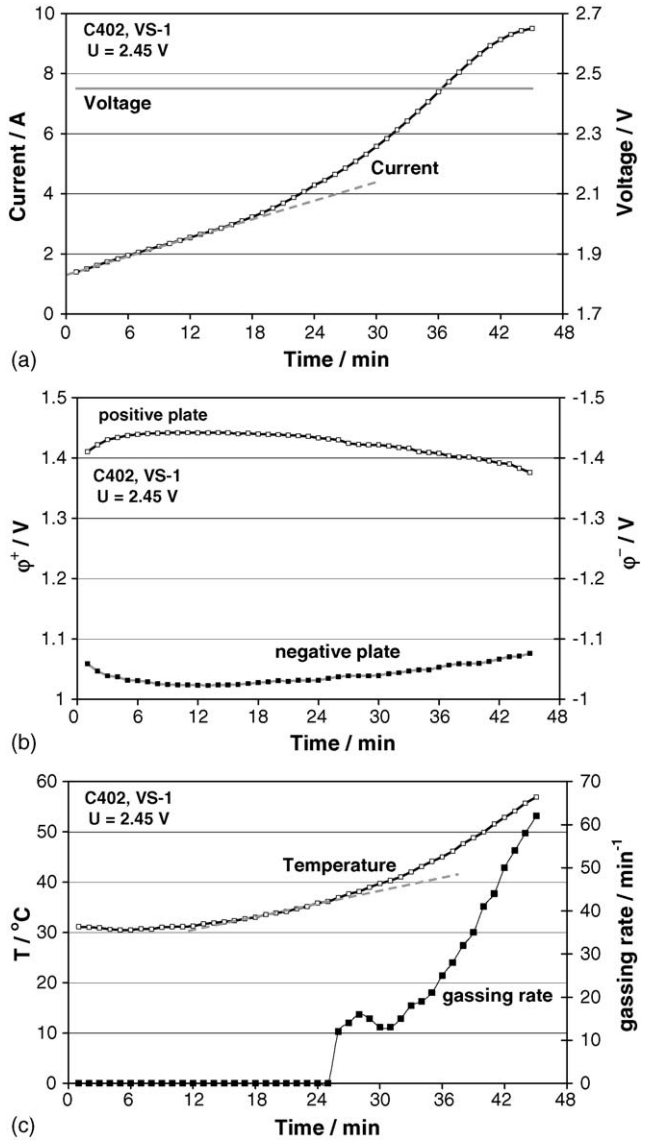

Fig. 3. Cell current (i), positive and negative plate potentials (φ^+ and φ^-), temperature (T) and gassing rate (dV_{out}/dt) vs. time of polarization (t) for sample cell C402, first voltage series VS-1, and $U = 2.45$ V.

Period A: When we start to polarize a fully charged cell, hydrogen and oxygen begin to evolve on the negative and positive electrodes, respectively. The electrode potentials versus Ag/Ag_2SO_4 are, respectively, −1.040 V and +1.360 V. Once oxygen is evolved, it passes through the separator and reaches the negative plate. Then a series of oxygen reduction reactions start at the negative electrode. These reactions reduce the absolute value of the negative electrode potential from 1.040 V to 0.98 V (see Fig. 5b). Since the voltage of the cell is kept constant, the potential of the positive electrode φ^+ must increase from 1.360 V to 1.420 V (Fig. 5a). The higher potential of the positive electrode leads to higher rate of the electrochemical reaction of oxygen evolution and hence the cell current increases from 0.7 A to 1.3 A. During period A, the master-electrode is the negative plate, while the slave-electrode is the positive plate.

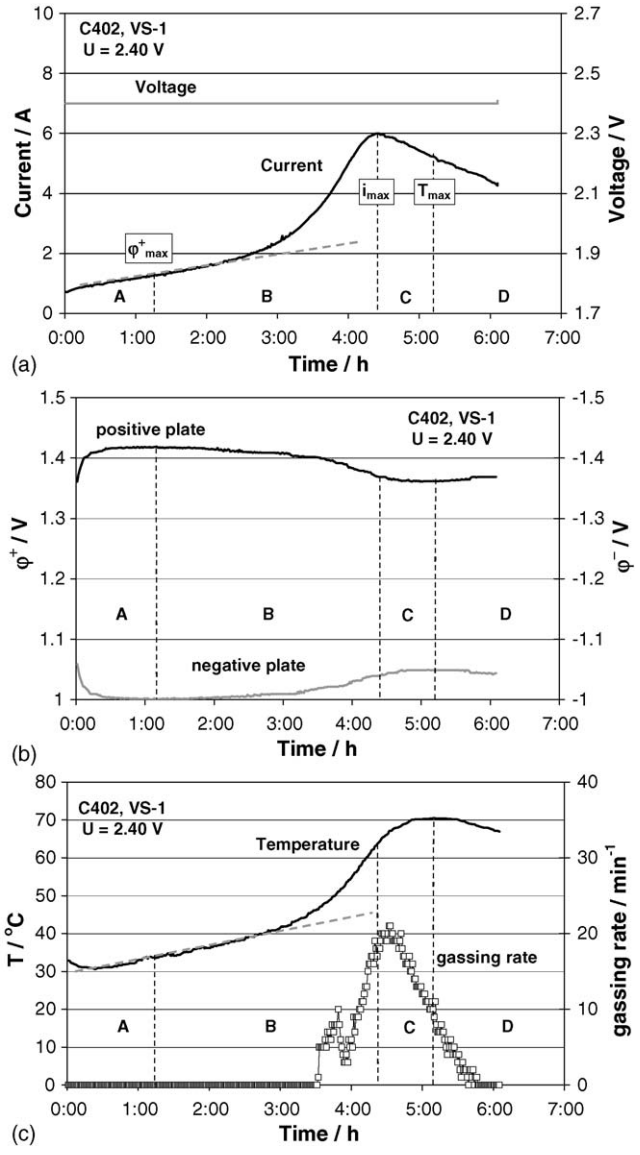

Fig. 4. Cell current (i), positive and negative plate potentials (φ^+ and φ^-), temperature (T) and gassing rate (dV_{out}/dt) vs. time of polarization (t) for sample cell C402, first voltage series VS-1, and $U = 2.40$ V.

Period B: When the reactions of O_2 reduction proceed at the negative plate, heat is released and the temperature starts to increase. At the positive plates, the overvoltage of O_2 evolution decreases and the current (the rate of O_2 evolution) increases. The latter accelerates the O_2 reduction at the negative plate, which in turn leads to generation of additional heat and further increase of the cell temperature. The above phenomena represent a Self-Accelerating Interrelation between the Reactions at the positive and negative Electrodes (SAIRE). The existence of this interrelation was reported in Ref. [12] and is illustrated in Fig. 6. The processes at the two electrodes are in *positive interrelation*, i.e. they accelerate each other.

On temperature rise, the heat flow from the cell to the surroundings increases, but the generated heat is still greater. The master-electrode during period B is the positive one and the slave-electrode is the negative one.

As evident from Fig. 5f, when $i = 3.4$ A the full amount of O_2 that is evolved on the positive plates cannot be consumed on the negative plate and part of the gas starts to leave the cell. Fig. 4c shows that the gassing rate and current reach their maximums close in time.

The experimental data evidence also that φ^+ and φ^- are linear functions of i and T during period B (see Fig. 5a and b).

$$\varphi^+ - \varphi^+_{max} = -9 \times 10^{-3}(i - i_{\varphi^+_{max}})$$

$$\varphi^- - \varphi^-_{min} = -9 \times 10^{-3}(i - i_{\varphi^-_{min}})$$

where $\varphi^+_{max} = 1.418$ V, $\varphi^-_{min} = -0.982$ V, and $i_{\varphi^+_{max}} = i_{\varphi^-_{min}} = 1.19$ A are the maximum and minimum values of the positive and negative plate potentials and of the current at φ^+_{max} (φ^-_{min}), respectively.

Period C: During this stage, the temperature rises from 64 °C to 72 °C, while the current decreases from 6 A to 5.4 A (Fig. 5a–d). The amount of electricity that flows through the cell during this period is 5 Ah. φ^+ continues to decrease, while φ^- increases. Because of the greater difference between the ambient temperature T_a and the temperature of the cell T (T_a is 23–25 °C and T rises from 62 °C to 70 °C), the rate of the heat flow leaving the cell increases and tends to cool the cell down. In addition, the lower current reduces the generated Joule heat. The linear dependences of φ^- and φ^+ on T (Fig. 5c and d) indicate that the amount of O_2 reduced at the negative electrode is approximately constant and the generated heat is equal to that during period B. The curves in Fig. 5e and f show that the decrease of i in period C affects mainly the amount of gas leaving the cell. In both periods B and C, φ^- and φ^+ are linear functions of T:

$$\varphi^+ - \varphi^+_{max} = -1.6 \times 10^{-3}(T - T_{\varphi^+_{max}})$$

$$\varphi^- - \varphi^-_{min} = -1.6 \times 10^{-3}(T - T_{\varphi^-_{min}})$$

where $T_{\varphi^+_{max}} = T_{\varphi^-_{min}} = 33.4$ °C is the temperature at φ^+_{max} (φ^-_{min}).

Since i decreases, the amount of O_2 reaching the negative electrode starts to decrease and at a certain moment, the sum of the heat generated by the reactions and the Joule heat becomes equal to the heat flown to the surrounding medium. At that moment, T reaches its maximum value T_{max}, which marks the end of period C.

Period D: Within this period, both the current and the temperature decrease with time. The lower current flowing through the cell causes a smaller amount of oxygen to be evolved at the positive plate. Therefore, less oxygen is reduced at the negative electrode and thus less heat is generated there per unit time. The amount of heat leaving the cell becomes greater than the sum of the heat generated by the reactions and the Joule heat, and hence the cell temperature decreases. Consequently, the rate of the reactions of oxygen evolution at the positive plate slows down. Thus, a *negative feedback* is established between the reactions taking place at the positive and negative plates, and they decelerate each other.

The self-decelerated interrelation between the reactions at the two electrodes continues until the heat leaving the cell per unit

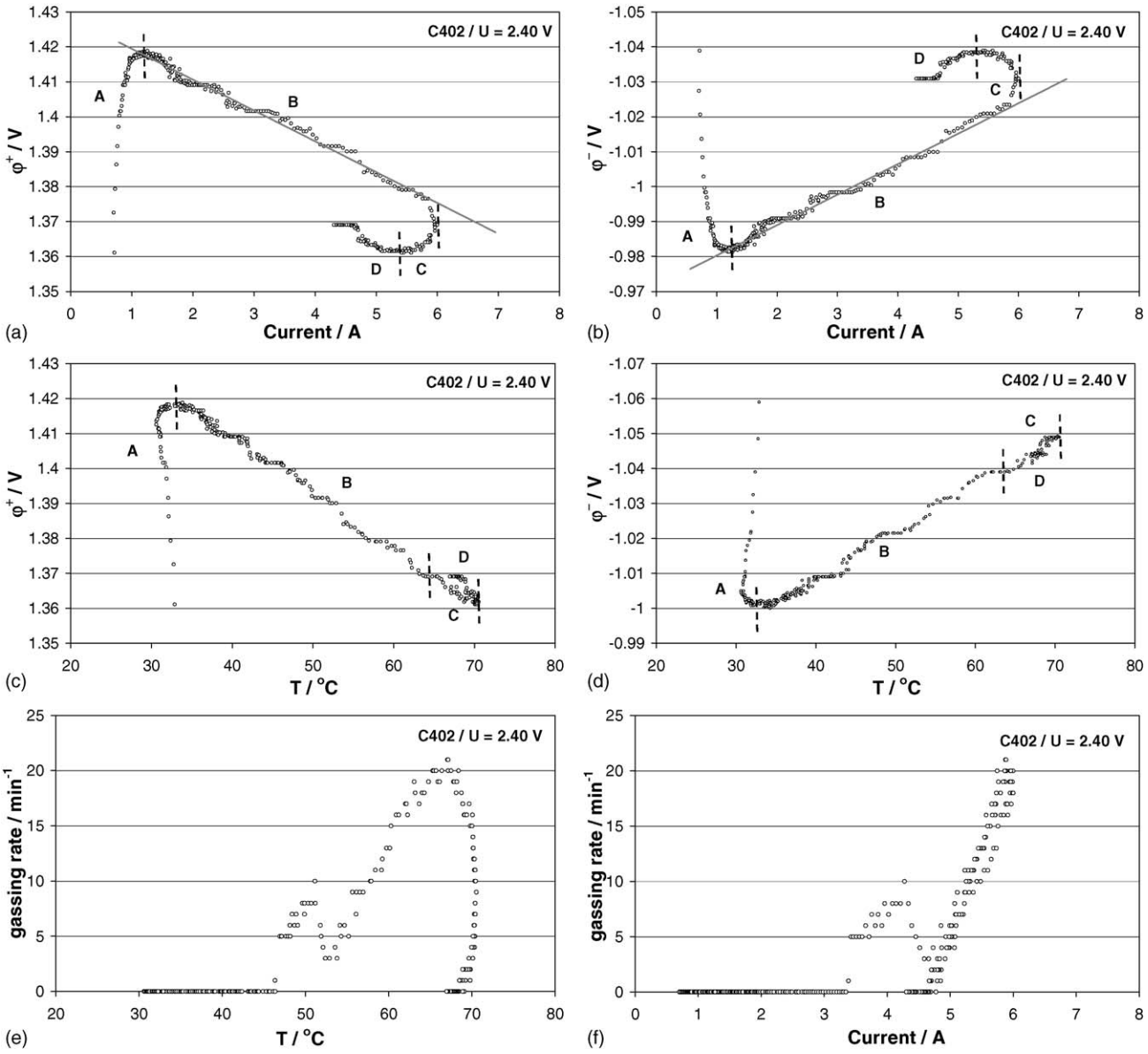

Fig. 5. Dependence of positive and negative plate potentials, and gassing rate on current and temperature for $U = 2.40$ V. The dashed lines mark the margins of the four periods in the development of the TRA phenomenon.

time equals the sum of the heat generated by the reactions and the Joule heat. Then, T and i reach their stationary values. This point marks the end of period D and the oxygen cycle starts to operate at steady-state regime.

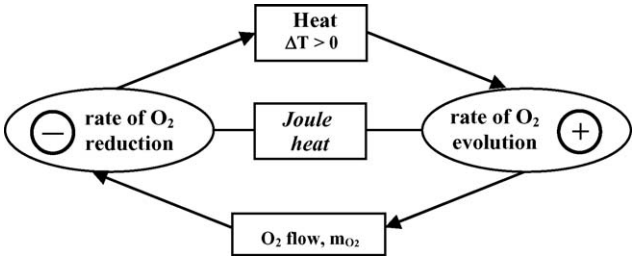

Fig. 6. Schematic representation of the self-accelerating interrelation between the reactions of the oxygen cycle at the two electrodes [12].

3.3. Influence of cell history on thermal runaway effect

We assume that the current maximum i_{max} (Figs. 4 and 5a, b) appears due to passivation of the positive plate, which limits further increase of i. The passivation is associated with structural changes in the PbO_2 active mass. These changes are partly irreversible and create a "memory" of the system's history. This memory should influence every subsequent polarization run of the same cell.

In an attempt to verify this hypothesis we performed subsequent experiments with the same test cell C402. This cell was polarized at six different voltages starting from 2.65 V down to 2.40 V through 50 mV. The polarization was stopped either when i reached 9.5 A or when T and i passed through maximums and reached stationary values. When this series was completed another two were performed following the same procedure.

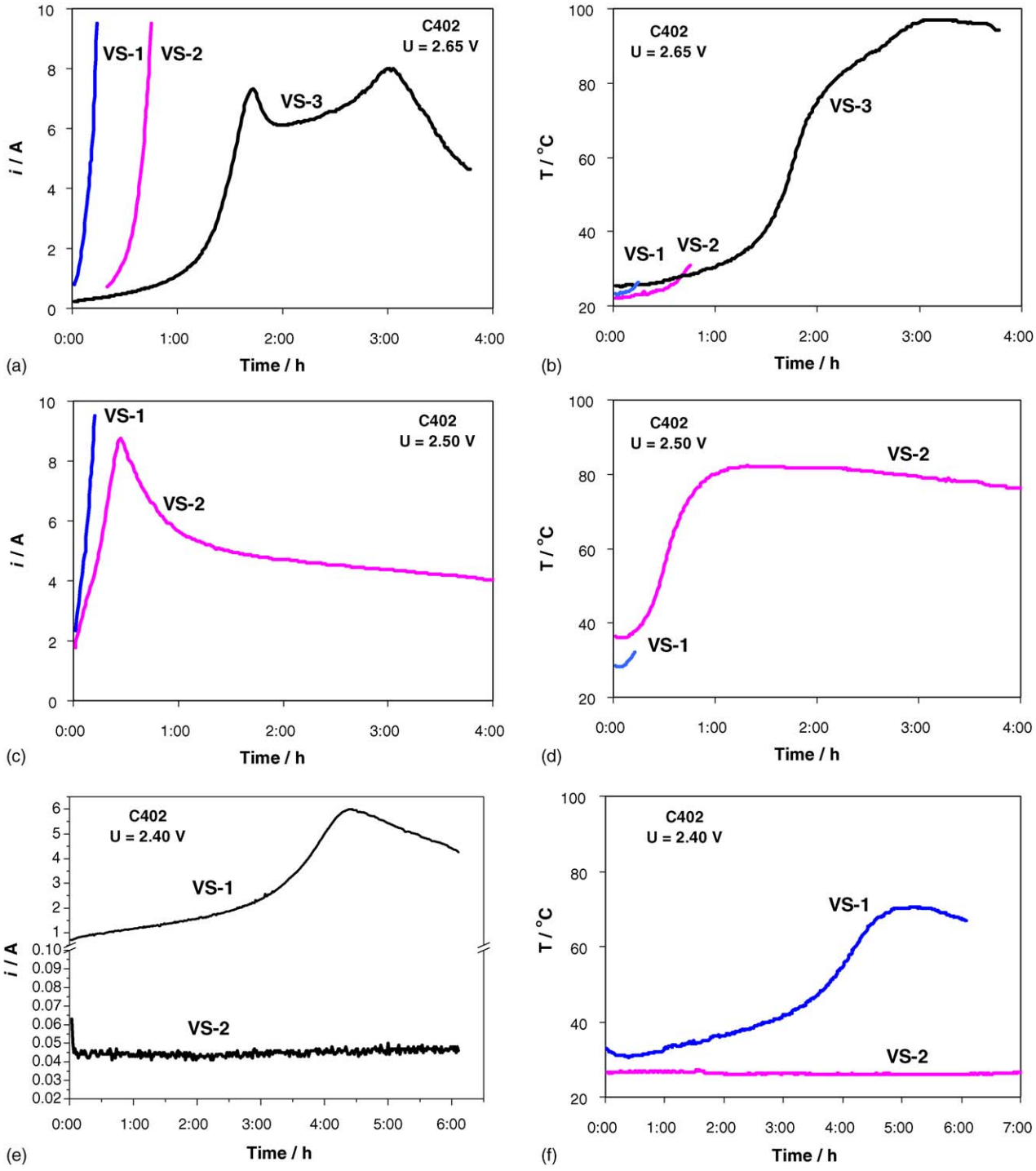

Fig. 7. Changes of current and cell temperature for voltage series VS-1, VS-2, and VS-3, at constant voltage polarization: (a and b) $U = 2.65$ V, (c and d) $U = 2.50$ V, and (e and f) $U = 2.40$ V.

Some of the results for the variations of current and temperature with time are given in Fig. 7. VS-1, VS-2, and VS-3 designate, respectively, the first, second, and third voltage series of experiments. In the first series, the current and temperature maximums appear at $U = 2.40$ V, in the second series these maximums appear at $U = 2.50$ V, and in the third series at $U = 2.65$ V. These results demonstrate clearly the passivation phenomena that occur when the temperature and current reach high values. The concept of electrode passivation is supported also by the data for the variation of i with time for every subsequent run (compare VS-1, VS-2, and VS-3 in Fig. 7a, c, and e). At $U = 2.40$ V after 1 h of polarization, $i = 1$ A for VS-1 against $i = 45$ mA for VS-2 (Fig. 7e).

Fig. 7a and b demonstrates another interesting effect. At $U = 2.65$ V for VS-1, the current increases up to 9.5 A, but the temperature remains almost constant. A current of 9.2 A is equal

to $2.2C_{10}$ A. This phenomenon is also observed in the VS-2 curve: i reaches 9.5 A, while T increases only by 8 °C. During the third voltage series (VS-3), however, a different behavior is observed: the temperature increases significantly and i passes through two maximums ($i_{1,max} = 7$ A, $T = 70$ °C and $i_{2,max} = 8$ A, $T = 96$ °C). This implies that during the first voltage series the processes that take place do not generate heat. The increase in current is mainly related to the accelerated rate of the O_2 reduction reaction in which no heat or a very small amount of heat is released. The changes in the structure of the positive active mass (PAM) and the negative active mass (NAM) during the first voltage series (VS-1) affect the processes that occur during the second series. During VS-2, a small amount of heat is generated and T increases by 8 °C. However, the structural changes in PAM and NAM are more significant during VS-2. Hence, during the third voltage series, the reactions that proceed are mainly exothermic. In VS-3, considerable amount of heat is generated and the cell temperature rises up to 96 °C.

3.4. Dependence of temperature on current at constant voltage polarization

The major problem created by TRA is the cell temperature rise to very high values. If the temperature remains higher than 60 °C for some time, the following undesirable effects appear: (a) the expander in the negative plate disintegrates [26]; (b) water evaporation increases greatly (if $T > 100$ °C, the electrolyte may start to boil) and the concentration of H_2SO_4 may become higher than 5.3 M (1.30 g cm^{-3}), thus causing passivation of the positive electrode [27]; (c) at $T > 90$ °C, the battery case swells and may unseal; (d) when the electrolyte starts to boil, colloidal PbO_2 forms and may penetrate into the separator and create short circuits; (e) H_2S and SO_2 may form [16]. The major issue in controlling TRA is to restrict the temperature rise below $T_{lim} = 60$ °C.

Fig. 8 shows the temperature versus current dependences for different polarization voltages during VS-1, VS-2, and VS-3. The experimental set-up limits the current up to 9.5 A.

The four periods discussed above, which represent the different stages in the thermal runaway processes taking place in the cell, are marked on the curves. The data for $U \geq 2.45$ V correspond only to periods A and part of B (Fig. 8a). It can be seen that the temperature depends linearly on the current within the major part of region B. After point B_a (Fig. 8a), T starts to increase faster and i reaches its maximum, i_{max} at $U = 2.40$ V. The slopes of the linear regions in the T versus i curves in region B ($b = dT/di$) for VS-1 are summarized in Table 1. With increasing the cell voltage, the slope b decreases, which means that the temperature rise becomes less sensitive to the increase in current. Hence, the current increase at high polarization voltages is not a result of temperature rise, but is rather due to some other processes in the cell, e.g. increased rate of the electrochemical reactions of oxygen reduction and restricted participation of exothermic reactions in this mechanism.

Fig. 8b and c presents the T versus i curves at different polarization voltages for the second and third voltage series. The results evidence again a linear dependence of cell temperature

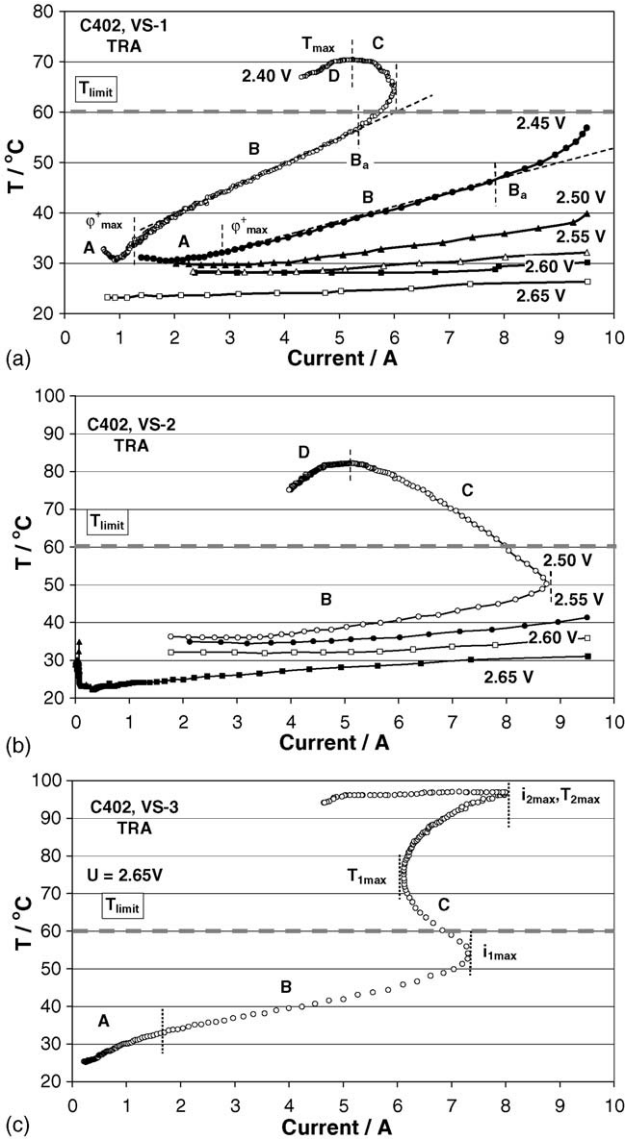

Fig. 8. Dependence of cell temperature on current for cell C402 with one layer of AGM separator for voltage series: (a) VS-1, (b) VS-2, and (c) VS-3.

on current in region B. In the third voltage series (2.65 V), a second maximum, $i_{max,2}$, appears. This more complex behavior is a result of subsequent reactivation of the electrodes during period C of the TRA phenomenon. For this run, when the temperature reaches 70 °C the current starts to increase reaching a second maximum at 8 A, which coincides with $T_{max} = 96$ °C.

Table 1
Slopes of the T vs. i curves for different polarization voltages in region B

Cell voltage, U	b
2.4	5.02
2.45	2.88
2.5	1.42
2.55	0.74
2.6	0.56
2.65	0.36

Comparing the results from the three subsequent series of experiments presented in Fig. 8 it can be concluded that, during the TRA phenomenon, T_{max} often appears at $T > 60\,^{\circ}C$ and only at $U = 2.40$ V, T_{max} is close to T_{lim} (Fig. 8a). Hence, the maximum polarization voltage should not exceed the value that keeps $T_{max} < 60\,^{\circ}C$. Unfortunately, this critical voltage depends on the history of the battery. Polarization voltage is only one of the parameters that can be used for controlling the TRA phenomena.

3.5. Influence of separator on TRA

The separator is the transport medium for O_2, H^+ ions, and H_2O. The separator/active masses interfaces are one of the regions where O_2 and H_2O fluxes are generated and consumed. Therefore, the geometry and structure of the separator should have significant effect on the TRA phenomenon. In order to investigate this effect we performed experiments with separators of different thickness and modified structure. The tests were performed following the same procedure as for cell C402 above.

First, we studied the influence of separator thickness. Fig. 9 presents the experimental data for three cells (C403, C404, and C405) assembled with two layers of AGM separator. The levels of compression and electrolyte saturation were varied.

Cell C405 was assembled applying the same compression and saturation level as with cell C402. The only difference was the thickness of the separator. It can be seen from Fig. 9c that TRA appears only at the highest voltage ($U = 2.65$ V). For all other polarization voltages, after the initial rise, the temperature reaches stationary value $T < 70\,^{\circ}C$. This means that the increased separator thickness suppresses TRA.

A comparison between Fig. 9a, b and Fig. 9a, c shows that at lower electrolyte saturation and higher compression the maximum in the current is lower, i.e. TRA is less pronounced.

In order to establish the influence of the separator nature (type) on TRA we performed a series of experiments on two cells (C406 and C407) with modified absorptive glass mat (MAGM) separator (detailed description of MAGM is given in Ref. [23]). The obtained experimental results are presented in Fig. 10. They indicate that TRA phenomena with temperature rise above 60 °C occur in cells C406 and C407 during VS-1 at 2.65 V. In all other cases, even if TRA does occur, the temperature does not exceed 60 °C and levels off at the end of the experiment, hence, the cells operate normally. The decrease in electrolyte saturation from 90% to 84% results in suppression of TRA. Our experiments demonstrate also that with every subsequent run, the maximum values of temperature and current decrease. As mentioned above, the possible reasons may be changes in the structure of the electrodes and the separator. In general, comparing Figs. 8 and 10 we can conclude that the TRA effects can be suppressed substantially if MAGM separator is used.

3.6. Teardown analysis of the active materials of cell C402 with single layer of AGM separator

Electrolyte: On completion of the tests, a severe electrolyte deficiency was observed throughout the separator volume. The

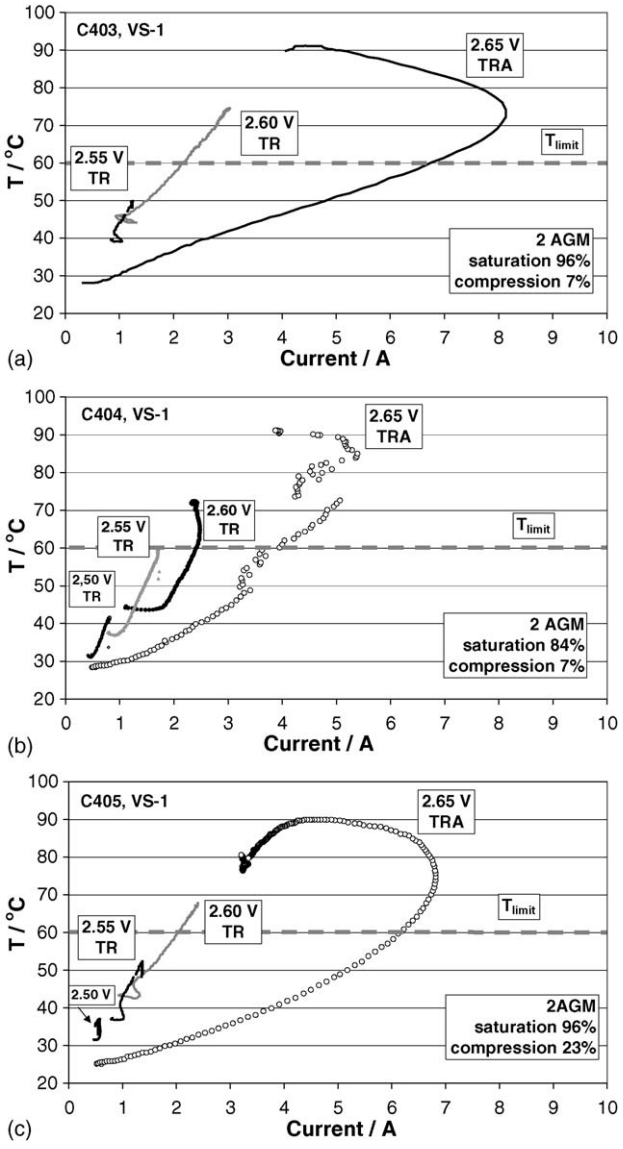

Fig. 9. Temperature vs. current curves for cells with two layers of AGM separator for VS-1: (a) cell C403, (b) cell 404, and (c) cell C405.

density of H_2SO_4 in the pores of the AGM separator was 1.33 g cm^{-3}. This value indicates that the PbO_2 electrode has undergone passivation [27], which is also evident from Fig. 7. Both the positive and negative plates seemed to be in good condition.

Phase composition of the active masses: The X-ray diffraction (XRD) patterns for positive active mass and negative active mass samples taken from the upper and lower parts of the plates are presented in Fig. 11. PAM is composed of β-PbO_2 with negligible amounts of $PbSO_4$ and α-PbO_2 as well. The content of $PbSO_4$ and α-PbO_2 in the bottom part of the cell is higher that in the upper part. NAM comprises Pb and about 33% $PbSO_4$ in the upper part of the plate, whereas in the bottom part the content of $PbSO_4$ is about 26% and additional amounts of 3BS and β-PbO are also detected.

Structure of the active masses: Photos of the micro- and macrostructure of PAM and NAM are presented in Fig. 12.

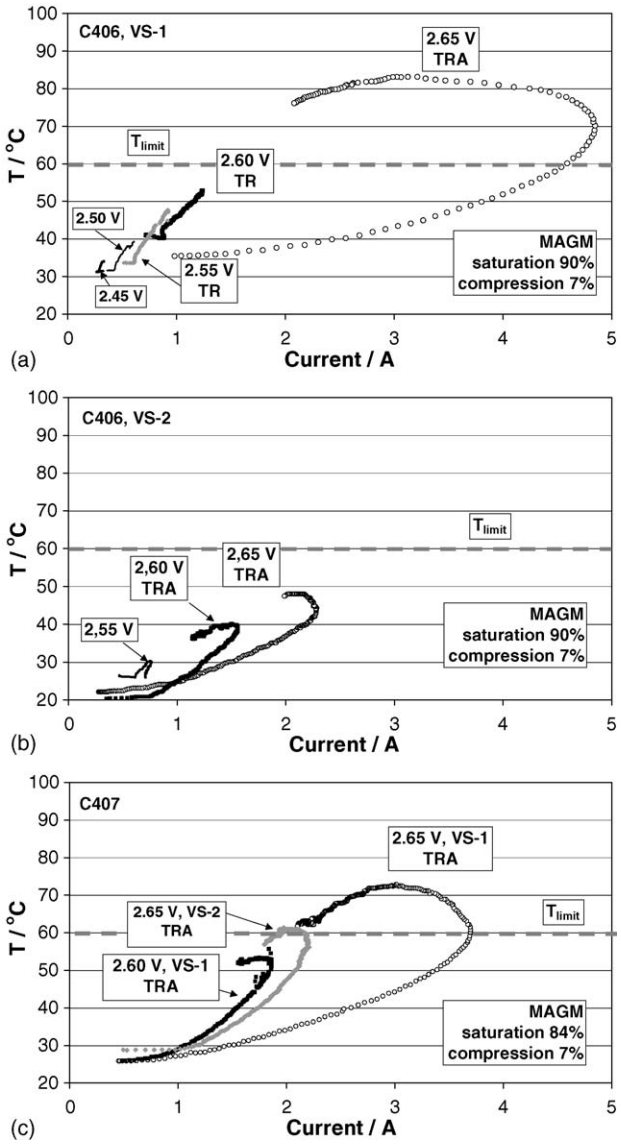

Fig. 10. Temperature vs. current curves for cells with one layer of MAGM separator: (a) cell C406 at VS-1, (b) cell C406 at VS-2, and (c) cell C407.

The positive active mass (PbO_2) is highly crystalline (Fig. 12b). The very high and sharp peeks for β-PbO_2 in the X-ray pattern (Fig. 11) confirm this crystalline structure of PAM. Fig. 12d features clearly 3BS and PbO particles on the Pb skeleton, which is also in agreement with the results of the XRD analysis.

3.7. Processes of oxygen evolution at the positive plate and its influence on the lead dioxide structure

The lead dioxide active mass is a complex system built up of particles and agglomerates containing zones of three different states that are in dynamic equilibrium [28,29]:

(a) crystal zone—composed of α- or/and β-PbO_2 crystals;
(b) amorphous zone—comprising amorphous lead dioxide;
(c) hydrated zone—PbO_2 interacts with water and forms $PbO(OH)_2$ or H_2PbO_3; hydrated zones are in equilibrium with cations and anions in the solution and the other two zones.

The changes in positive plate potential and in amount of lead dioxide crystals in the active mass during overcharge were determined in Ref. [28] and they are presented in Fig. 13. When the charged cell is left on open circuit, φ^+ decreases while the crystallinity of PbO_2 particles increases. During overcharge (oxygen evolution), φ^+ increases rapidly and the crystallinity of PbO_2 decreases. These results suggest that O_2 evolution influences not only the electrode potential, but also the amount of the lead dioxide crystals in the active mass.

There are two mechanisms of oxygen evolution. In the first one, PbO_2 is not involved and this mechanism consists of the following elementary reactions:

$$H_2O \rightarrow OH + H^+ + e^- \quad (1)$$

$$2OH \rightarrow O + H_2O \quad (2)$$

$$2O \rightarrow O_2 \quad (3)$$

For the second mechanism, it is assumed that the oxygen evolution reaction proceeds in active centers in the hydrated zones. The following elementary reactions take place [13]:

$$PbO^*(OH)_2 \rightarrow PbO^*(OH)^+ + OH + e^- \quad (4)$$

$$PbO^*(OH)^+ + H_2O \rightarrow PbO^*(OH)_2 + H^+ \quad (5)$$

$$OH \rightarrow O + H^+ + e^- \quad (6)$$

$$2O \rightarrow O_2 \quad (3)$$

$PbO^*(OH)_2$ denotes an active center in the hydrated (gel) zone. The number of active centers depends on the structure and volume of the hydrated zone.

Regardless of the type of mechanism of the oxygen evolution reactions, O_2 molecules, O atoms, and OH radicals are formed. They diffuse into the PbO_2 particles and agglomerates creating great number of defects in these crystal PbO_2 zones, thus transforming them into amorphous zones. This process is clearly demonstrated in Fig. 13. When the O_2 evolution reaction stops, the above oxygen particles migrate out of the solid phase causing partial or complete restoration of the crystal zones and consequently, the electrode potential declines (Fig. 13).

It has been established that the PbO_2 conductivity depends on its non-stoichiometry [30]. $PbO_{1.74}$ has the highest conductivity, while the conductivity of $PbO_{1.92}$ is an order of magnitude lower. With incorporation of OH, O, and O_2 into the crystal lattice, Pb^{2+} ions in these non-stoichiometric oxides oxidize and over-stoichiometric oxygen may be formed. Hence, it can be expected that the conductivity will decrease.

With increase of temperature, the rate of the oxygen evolution reaction increases, too. This will continue until the volume of the hydrated zones starts to decrease. Fig. 12 shows that PbO_2 particles have crystal form. This means that α-PbO_2 and β-PbO_2 give the form of the particles and the hydrated zones have shrunk and do not affect the particles' shape. Hence, the number of active centers in which O_2 evolution proceeds also decreases

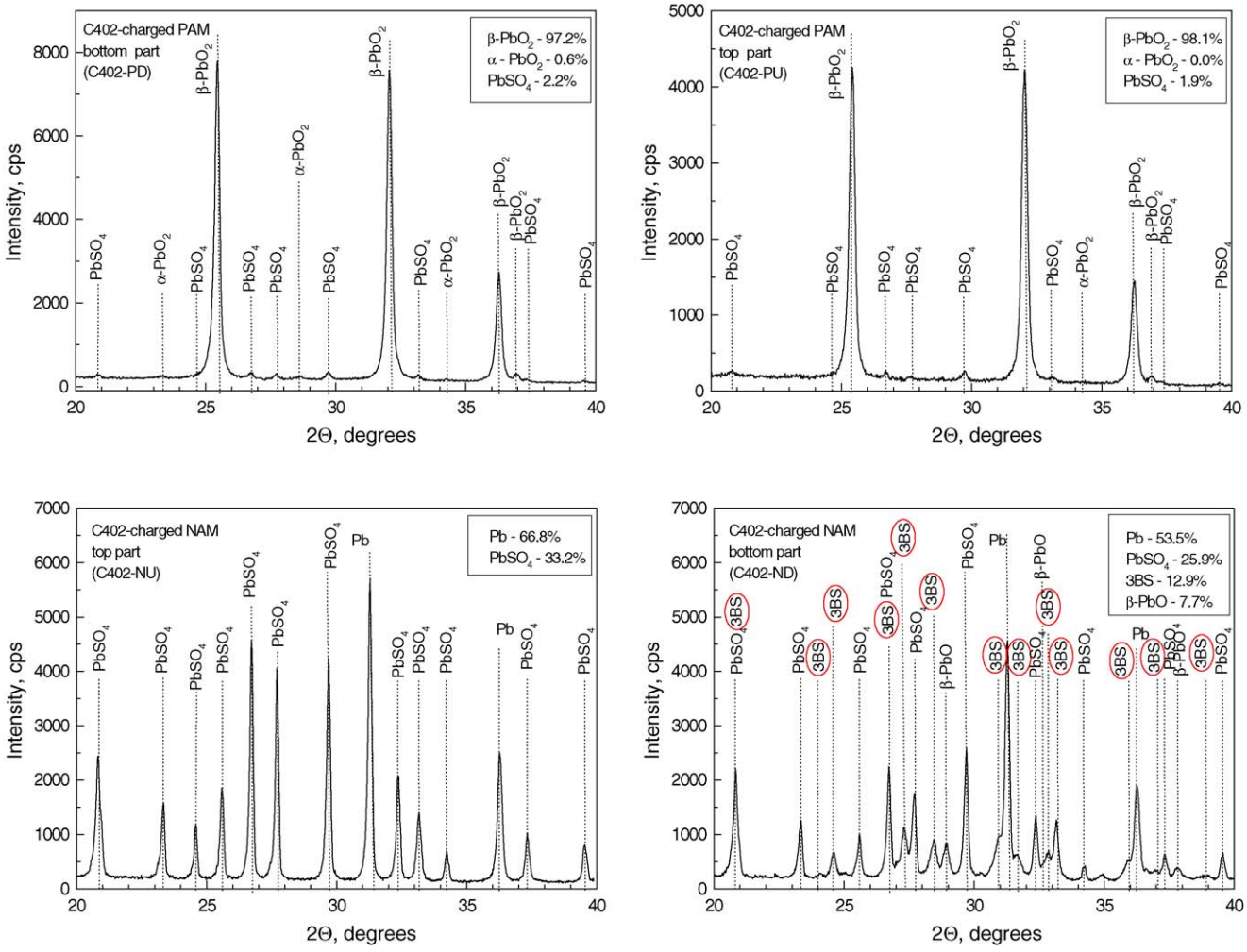

Fig. 11. X-ray diffraction (XRD) patterns for samples from the top and bottom parts of the positive and negative plates of AGM cell.

with decrease of the volume of the hydrated zones. Due to these structural changes, the rate of the oxygen evolution reaction reaches a maximum and then decreases thereafter. These phenomena are illustrated in Figs. 4 and 7.

It has been established that for temperatures higher than 60 °C the volume of the crystal zones is five times larger than that at 20 °C [14]. Probably, at these high temperatures, the structural changes in PbO_2 particles and agglomerates are irreversible and a 'memory' is created in the system. This conjecture is confirmed by the experimental results in Fig. 7: i_{max} decreases for every subsequent voltage series. Hence, i_{max} depends on the structural changes in PbO_2, which in turn depend on temperature.

The composition of the hydrated zones depends also on the concentration of H_2SO_4. Hydrated zones and the solution exchange ions, and the following reactions proceed [31]:

$$PbO(OH)_2 + H_2SO_4 \rightleftarrows PbOSO_4 + H_2O \quad (7)$$

$$PbO(OH)_2 + 2H_2SO_4 \rightleftarrows PbO(HSO)_4 + 2H_2O \quad (8)$$

It is well known from the literature that the lead dioxide active mass absorbs readily SO_4^{2-} and HSO_4^- ions [32,33]. Due to this process, the concentration of active centers in the hydrated zones decreases, which slows down the rate of O_2 evolution.

During operation of the oxygen cycle, water is consumed at the positive plate and the concentration of H_2SO_4 at the separator/positive active mass interface increases. This leads to sulfation of the hydrated zones, which is the second factor responsible for the reduced rate of the oxygen evolution reaction and for passivation of the lead dioxide active mass.

3.8. Chemical and electrochemical reactions of oxygen reduction at the negative plate

Oxygen reduction may proceed through several mechanisms at the negative electrode, depending on the conditions.

3.8.1. Electrochemical mechanism of O_2 reduction

According to this mechanism the following reaction proceeds:

$$O_2 + 2H^+ + 2e^- \rightarrow H_2O_2 \quad (9)$$

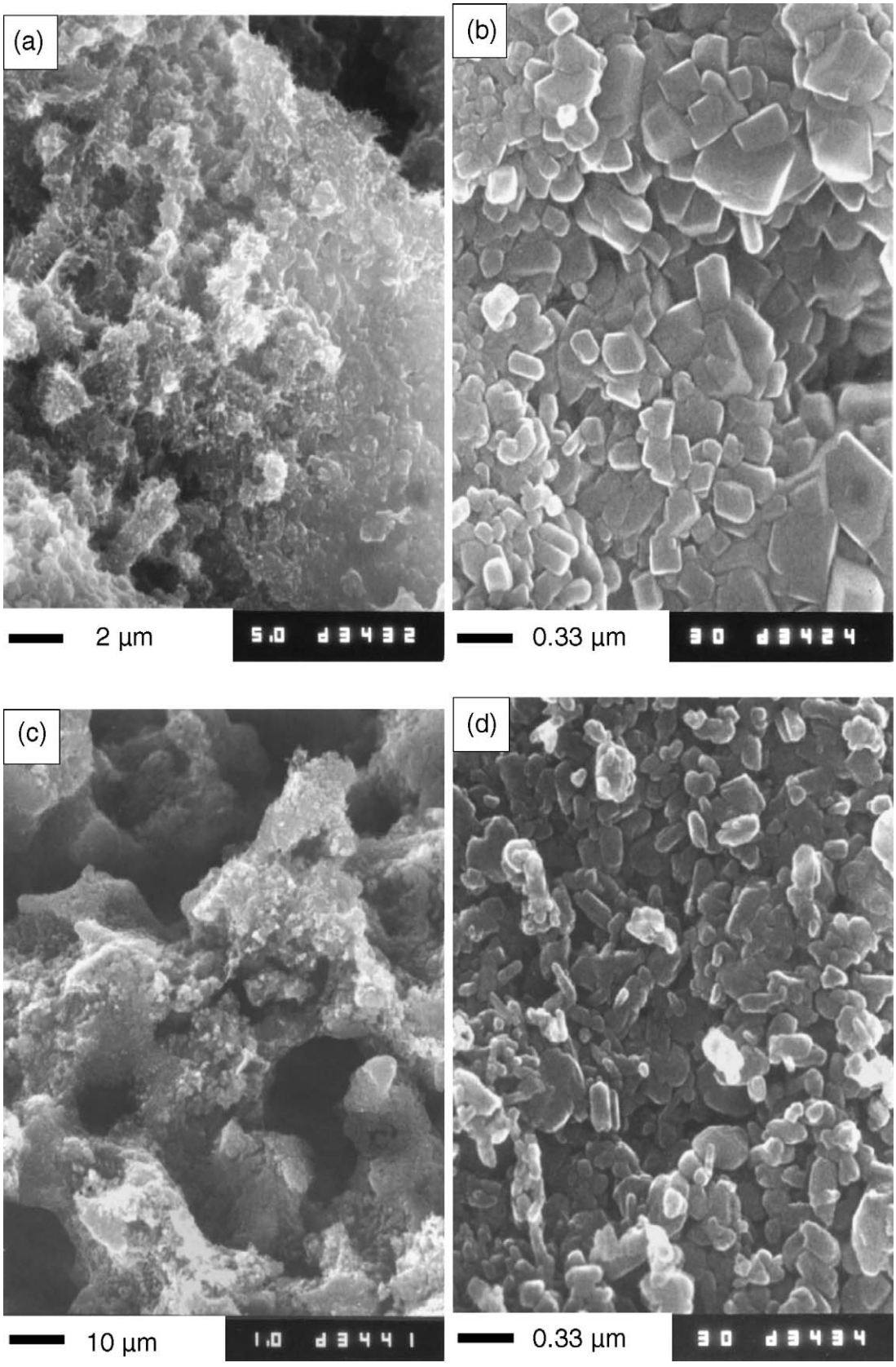

Fig. 12. Scanning electron microscopy results for fully charged cell C402: (a) macrostructure of PAM, (b) microstructure of PAM, (c) macrostructure of NAM, and (d) microstructure of NAM.

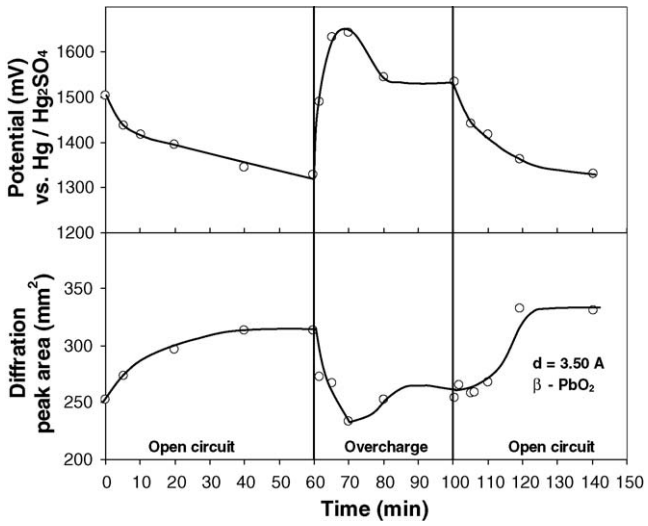

Fig. 13. Changes in potential and intensity of the X-ray diffraction line 3.50 Å for β-PbO_2 on open circuit and during overcharge.

This reaction has been found to be fast and to proceed when oxygen is reduced on Hg substrate [34], Ag–Au [35,36], Ag–Cu–Hg [37], Au [38], Pt and platinated Pt [39], and Ni [40]. There is no reason to assume that Pb will be an exception. The formation of H_2O_2 on oxygen reduction has been established through the reduction of O_2 enriched with ^{18}O isotope [41]. The same percent contents of ^{18}O–^{18}O and ^{18}O–^{16}O have been found in H_2O_2 as in the initial (primary) oxygen. Hence, the conclusion has been drawn that the O–O bond in the oxygen molecule does not break during reduction of O_2 to H_2O_2.

Once formed, H_2O_2 may reduce by electrochemical mechanism:

$$H_2O_2 + 2H^+ + 2e^- \rightarrow 2H_2O \quad (10)$$

This reaction proceeds at considerable overvoltages and has been investigated for Hg [34], Pt [39], and gold [38] substrates. It has been established that the reduction involves non-dissociated H_2O_2 molecules and is slow.

3.8.2. Chemical mechanism of H_2O_2 reduction with involvement of hydrogen [15]

Parallel to reaction (9), a reaction of hydrogen evolution proceeds at the lead surface:

$$2H^+ + 2e^- \rightarrow 2H \quad (11)$$

Hydrogen atoms are a strong reducer and H_2O_2 is a strong oxidizer. Both products are formed simultaneously at the lead surface. Part of the evolved hydrogen $(1-\theta)$H reacts with H_2O_2 through the following chemical reaction:

$$2(1-\theta)H + (1-\theta)H_2O_2 \rightarrow 2(1-\theta)H_2O + (-(1-\theta) \times 383.88\,\text{kJ mol}^{-1}) \quad (12)$$

It has been shown experimentally [15] that this reaction proceeds at the negative plate during the oxygen cycle.

Another part of hydrogen (θ) forms molecules and leaves the cell together with an equivalent amount of oxygen that has not reacted by reaction (9). The rate of this gas flow is measured with the help of a flowmeter.

$$2\theta H \rightarrow \theta H_2 \quad (13)$$

The ratio between the rates of reactions (12) and (13) determines the efficiency of the oxygen cycle. If the rate of reaction (12) is much higher than that of reaction (13), the efficiency of the oxygen cycle is high and vice versa. So, the oxygen cycle is an open system and parts of O_2 and H_2 leave the cell through the valve.

3.8.3. Chemical reaction between H_2O_2 and Pb

H_2O_2 oxidizes the lead surface through the following chemical reaction:

$$H_2O_2 + Pb \rightarrow PbO + H_2O + (-317.04\,\text{kJ mol}^{-1}) \quad (14)$$

Further, PbO may be reduced to Pb through the electrochemical reaction:

$$PbO + 2H^+ + 2e^- \rightarrow Pb + H_2O \quad (15)$$

whereby water is formed and the lead surface is rebuilt.

However, PbO may also react with H_2SO_4 forming $PbSO_4$:

$$PbO + H_2SO_4 \rightarrow PbSO_4 + H_2O + (-77.51\,\text{kJ mol}^{-1}) \quad (16)$$

$PbSO_4$ is reduced to Pb through the electrochemical reaction of charge at the negative plate:

$$PbSO_4 + 2H^+ + 2e^- \rightarrow Pb + H_2SO_4 \quad (17)$$

Reactions (15) and (16) are in competition. Reaction (17) may proceed at low rate and, though the plate is charged, certain amounts of $PbSO_4$, PbO, and basic lead sulfates may form in the negative active mass as a result of reactions (14) and (16). These are indeed detected by XRD analysis (Fig. 11). This indicates that the negative plate is partially discharged during the OxCy.

3.8.4. Chemical mechanism of oxygen reduction through oxidation of the lead surface

The evolved oxygen oxidizes the lead surface:

$$O_2 + 2Pb \rightarrow 2PbO + (-219\,\text{kJ mol}^{-1}) \quad (18)$$

Then, PbO may be reduced through the electrochemical reaction (15) or be sulphated (reaction (16)) and the obtained $PbSO_4$ may then be reduced through reaction (17).

All chemical reactions involved in the above mechanisms are associated with heat release. Depending on the conditions at the negative plate/separator interface, the reactions will compete with each other.

3.9. Calculation of the thermal balance in the cell

In order to estimate the thermal effects caused by the chemical and electrochemical reactions, we calculated the generated and Joule heat for our cell C402.

For a single cell with immobilized electrolyte and small thickness (small Biot number), the differential equation that describes the temperature distribution can be reduced to the lump-parameter model of energy balance, which takes the form [42]:

$$\frac{\partial(C_p T)}{\partial t} + hA_c(T - T_a) = q \tag{19}$$

where C_p is the cell thermal capacity, h the convective heat transfer coefficient, A_c the surface area of the cell, T_a the ambient temperature, T the cell temperature, and q is the heat generation rate. Integrating the above equation over time gives us the expression for the generated heat in the cell, Q:

$$Q = \int_0^t q\,\mathrm{d}t = C_p(T - T_{ref}) + hA_c \int_0^t (T - T_a)\,\mathrm{d}t \tag{20}$$

T_{ref} is the temperature of the cell at the beginning of the experiment. Q can be presented as a sum of the Joule heat (Q_J) that represents the conversion of electrical energy into thermal energy, and the heat generated by the chemical reactions (Q_r): $Q = Q_J + Q_r$.

If we know the resistance of the cell R, the Joule heat can be calculated from the expression:

$$Q_J = \int_0^t Ri^2\,\mathrm{d}t \tag{21}$$

For our sample cell C402, $C_p = 293\ \mathrm{J\ K^{-1}}$ and $R = 57.8\ \mathrm{m\Omega}$. The value for the convective heat transfer coefficient was chosen to be $h = 5\ \mathrm{W\ m^{-2}\ K^{-1}}$, which is the value for free-air convection [42].

Fig. 14 presents the calculated values for the total generated heat (Q), the heat generated by the chemical and electrochemical reactions (Q_r), and the Joule heat (Q_J) as a function of time for cell C402 at $U = 2.40$ V, 2.50 V, and 2.65 V, VS-1. The results for $U = 2.40$ V (Fig. 14a) suggest that during the whole experiment the major part of the generated heat is due to the chemical and electrochemical reactions that proceed in the cell. The Joule effect becomes significant after 4 h of polarization, when the cell current is high enough. It can be seen from Fig. 14a that, in the beginning of the experiment (region A), the generated heat is almost equal to the reactions heat. We can assume that in the very beginning, Q is equal to the heat released mainly by the electrochemical reduction of O_2. Then, a self-accelerating interrelation between the reactions at the two electrodes sets up and the generated heat increases linearly with time (region B up to α). When the temperature rises, the hydrogen over-potential decreases. More hydrogen is evolved which takes part in reaction (12) of H_2O_2 reduction. Reaction (12) is associated with generation of a great amount of heat, which leads to rapid temperature rise in the cell. This is illustrated in Fig. 14a, in the region between α and β on the Q_r curve. This process contributes further to the self-accelerating interrelation between the reactions at the two electrodes. Probably, parallel to the above chemical mechanism, reactions of chemical oxidation of Pb may take place, too (reactions (14)–(18)). The PbO_2 electrode undergoes passivation (Fig. 4) and i starts to decrease. After point β

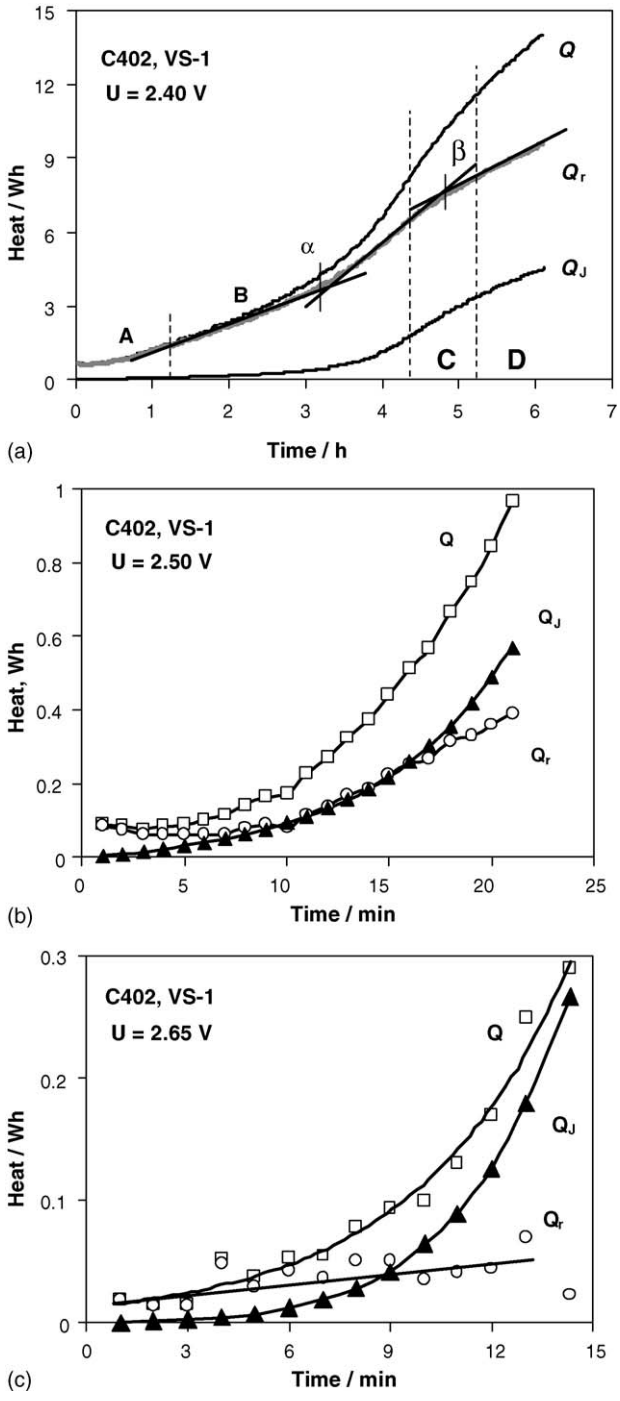

Fig. 14. Changes in generated heat (Q), reactions heat (Q_r), and Joule heat (Q_J) during polarization of cell C402, VS-1, at: (a) $U = 2.40$ V, (b) $U = 2.50$ V, and (c) $U = 2.65$ V.

(Fig. 14a), the heat generated by the reactions starts to decrease and the $\mathrm{d}H/\mathrm{d}t$ slope declines.

For $U = 2.65$ V (Fig. 14c), the opposite situation is observed. As can be seen from Fig. 7a and b, the current reaches the maximum allowed value of 9.5 A very quickly, while the temperature increases but slightly. Fig. 14c shows that this slight increase in temperature is mainly due to Joule effects. The heat effect of the reactions that proceed at $U = 2.65$ V is very small and contributes an insignificant part to the total heat generated in the cell

up to 12 min. These results imply that the O_2 reduction at the negative plate proceeds through an electrochemical mechanism (reactions (9) and (10)). This is due to the high voltage applied, which strongly polarizes the electrodes. When the O_2 reduction processes are electrochemical, the chemical energy (enthalpy) of the system converts into electrical energy and only a small part may be released as heat.

Fig. 14b indicates that at $U = 2.50$ V (VS-1), initially (for about 7 min) the heat effect of the reactions (Q_r) is greater than the Joule heat effect. Then, between the 7th and 18th minutes, the two effects become equal, and after that the Joule heat effect predominates over the reaction heat effect, due to the substantial current increase (Fig. 14b). Obviously, at this cell voltage and as a result of the passivation of the Pb and PbO_2 electrodes, the mechanism of O_2 reduction at the negative plate changes involving, beside the electrochemical reactions, also exothermic chemical reactions. That is the reason for the greater amount of heat released in the cell as compared to that on polarization of the cell at 2.65 V (Fig. 14c).

3.10. Types of thermal phenomena and their evolution

Through varying the value of the constant voltage applied to the cell and the type and thickness of the separator used, we investigated the various thermal phenomena proceeding in the VRLA cell. These phenomena manifest through the changes in two basic parameters: cell temperature and current. The relation between these parameters is presented in Figs. 8–10. Judging by the profile of the *T*/*i* curves, the intensity of the heat effects can be divided in three regions:

(a) Phenomena due to the spontaneous current increase above $i > 2C_{10}$ A and appearance of i_{max} in this region. In our investigations, the current was limited to $i = 2C_{10}$ A, thus preventing the thermal phenomena to proceed. The behavior of *i* and *T* within this current region $i < 2C_{10}$ A is illustrated in Figs. 8a, b and 14c. It is determined by the high polarization voltage of a new cell with non-passivated Pb and PbO_2 electrodes, and a thin AGM layer (with low ohmic resistance and thermal capacity). Fig. 7a (VS-1) shows that *i* increases rapidly, which is due to the increased number of gas channels in the AGM separator. The flow of O_2 passing through the separator is intensified and it is reduced at the non-passivated Pb surface. Only a small temperature rise is observed, which indicates that reduction of oxygen proceeds through electrochemical reactions (9) and (10). The increase in cell temperature is a result mainly of the Joule effect (Fig. 14c).

Polarization of this cell was interrupted when the current reached a value $I = 9.5$ A ($i = 2C_{10}$ A), so as to avoid further current increase and thus to prevent intensive development of the TRA phenomena, which might cause battery damage.

(b) Phenomena leading to spontaneous current increase reaching maximum values $1C_{10}\,A < i_{max} < 2C_{10}\,A$ at U = constant. The thermal phenomena that proceed within this region cause maximum temperature increase up to and above the upper temperature limit for normal battery operation. Only in single cases may i_{max} reach the boiling point of the electrolyte (self-activation, Fig. 8c). The heat effects within this region may exhibit when the Pb and PbO_2 electrodes are partially passivated and when separators of medium thickness are used. In this region, T_{max} reaches values up to 70–90 °C, whereas *i* is limited by the passivation of the PbO_2 electrode. The reduction of oxygen involves exothermic chemical reactions which contribute mostly to the generated heat in the cell (Figs. 8, 9, and 14a). Within this region of intensity of the thermal phenomena, the TRA proceeds through all four stages of its development, but not very intensively. Hence, most often no damage is caused to the battery, except for single cases of re-activated electrodes.

(c) Phenomena resulting in spontaneous current increase only up to a maximum of $i_{max} < 1C_{10}$ A. The thermal phenomena within this region do not lead to temperature rise above the upper temperature limit of normal battery operation, $T_{max} < T_{lim}$. These phenomena proceed when (a) the polarization voltage of the cell is low, (b) Pb and PbO_2 electrodes have definite structure and/or are partially passivated, and (c) the thickness of AGM separator exceeds given value or AGM separator has given properties and structure. In this case the thermal capacity of the cell is significant and more heat is needed to increase the cell temperature. The temperature increase within this region is mainly due to exothermic chemical reactions. In this case, the TRA develops through all four stages, but within the temperature range of normal battery operation and hence, has not harmful effect in the battery (Fig. 10).

Figs. 7 and 14 show that the thermal phenomena undergo an evolution during battery operation, one mechanism of the reactions of oxygen reduction being replaced by another one, depending on the changes in the Pb and PbO_2 electrodes.

The margins of the above distinguished current regions of thermal intensity are not absolute. They will depend on the Ah capacity and on the design of the battery as well as on the temperature heterogeneity within the cell volume.

4. Summary

On grounds of the experimental results and the proposed chemical and electrochemical reactions that take place at the two electrodes, a unified model for the phenomena proceeding during OxCy operation can be proposed. This model is represented schematically in Fig. 15.

In VRLA batteries, two electrochemical systems operate: (A) lead current generating and accumulating system and (B) oxygen cycle. The electrodes of the lead system (Pb and PbO_2) serve also as electrodes of the oxygen cycle. The two systems are interrelated and are in mutual dependence. On PbO_2 electrode water is formed and O_2 is released. The concentration of H_2SO_4 increases. The reaction of O_2 evolution proceeds in active centers in the hydrated zones of the lead dioxide electrode. The number of active centers depends strongly on electrolyte concentration and temperature. Oxygen reduction with water formation takes

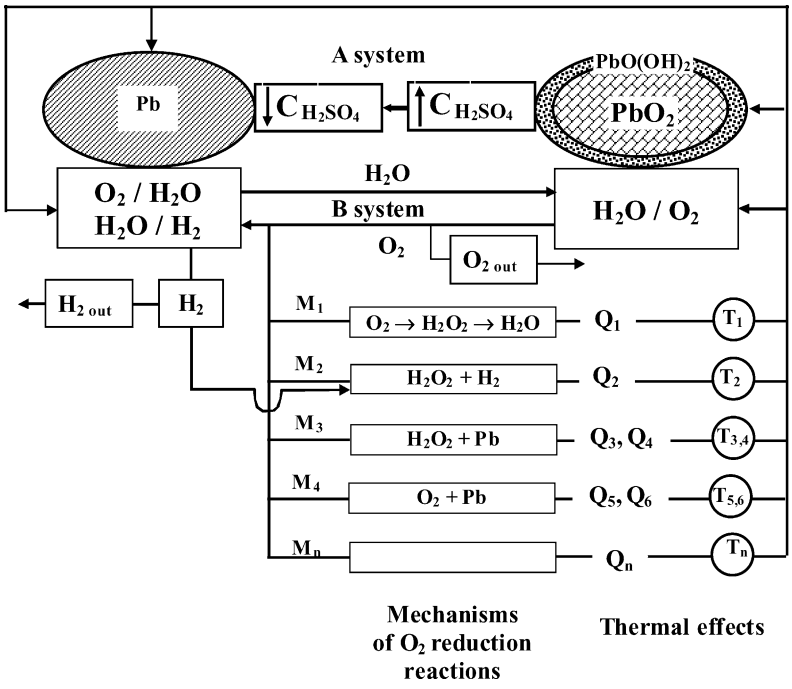

Fig. 15. Scheme of the processes that take place during oxygen cycle operation. Depending on the structure of the active masses and the conditions of cell operation, O_2 reduction proceeds through several mechanisms at the negative plate. Due to their exothermic effects, the cell temperature increases, which affects the structure of the Pb and PbO_2 electrodes and all processes involved in the OxCy.

place at the lead electrode surface and H_2SO_4 concentration at this surface decreases. Hydrogen is evolved at the same surface. These reactions depend on the adsorption of the expander and the degree of oxidation of the lead surface. Electrolyte concentration and temperature also affect the condition of the lead surface. Parts of Pb surface can be covered with lead compounds.

The rise in cell temperature is mainly due to O_2 reduction at the negative plates, which may proceed through different mechanisms (M_1, M_2, ..., M_n). In the present work, we propose four mechanisms. When the oxygen is reduced through electrochemical reactions only (mechanism M_1), the released heat (Q_1) is very small. Hence, the cell temperature rises mainly due to Joule heat effects. More often, however, exothermic chemical reactions are involved in the O_2 reduction. We propose three analogous mechanisms (M_2, M_3, and M_4), but probably there are others, too. When the reactions proceed through these mechanisms, the released heat (Q_2–Q_6) is significant. Involvement of these chemical reactions leads to rapid increase in temperature (T_2–T_6). The elevated temperature will affect the structure of the Pb and PbO_2 electrodes, and the rates of O_2 evolution at the positive plate (H_2O/O_2 reaction) and H_2 evolution as well as of O_2 reduction at the negative plates (H_2O/H_2 and O_2/H_2O reactions). Consequently, the mechanism of the reactions undergoes evolution.

In order to avoid appearance of TRA effect with high temperature values, $T_{max} > T_{lim}$, and disastrous effect on the battery the following steps must be taken into account:

(a) The battery separator should be chosen with the appropriate thickness, structure of the AGM sheet and nature of the silica fibers. The latter can be achieved by treatment of the separator with polymer solution. The increase of the separator thickness leads to increase of the amount of the electrolyte and hence causes increase of the thermal capacity and slows down the rate of temperature rise.
(b) The applied voltage during float or overcharge should not exceed certain critical value. Present investigations show that after given period of exploitation (after which PbO_2 and Pb electrodes are partially passivated) this critical value may increase without causing any damages of the battery.
(c) In order to secure the battery long life the current during overcharge should be limited up to $1C_{10}$ A.
(d) It may be possible by adding certain additives to the negative active mass to prevent its undesirable changes which favor proceeding of exothermic chemical reactions. Such additives should accelerate reaction (10) and hence increase the reversibility of the oxygen cycle.

The mechanisms of the processes taking place during OxCy operation described above are complex, interrelated and causing thermal effects. With the present investigation, we have tried to reveal the nature of these processes and to suggest ways to suppress the undesirable effects by facilitating appropriate mechanisms of O_2 reduction associated with small amount of generated heat.

Acknowledgements

The authors are very grateful to Dr. H. Catherino for the helpful discussions and to the USA Army European Research Office, London, England, for the financial support provided for this work.

References

[1] D.H. McLelland, J.L. Devitt, U.S. Patent #3,862,861 (1975).
[2] S. Hills, D.L.K. Chu, J. Electrochem. Soc. 116 (1969) 1155.
[3] B.K. Mahato, E.Y. Weissman, E.C. Laird, J. Electrochem. Soc. 121 (1974) 13.
[4] H. Giess, J. Power Sources 67 (1997) 49.
[5] P. Haering, H. Giess, J. Power Sources 95 (2001) 153.
[6] A. Pesaran, M. Keyser, Thermal characteristics of selected EV and HEV batteries, in: Proceedings of the 16th Annual Battery Conference: Advances and Applications, Long Beach, CA, January 9–12, 2001.
[7] A. Pesaran, A. Vlahinos, S.D. Burch, Thermal performance of EV and HEV battery modules and packs, in: Proceedings of the 14th Electric Vehicles Symposium, Orlando, FL, December 12–17, 1997.
[8] A. Pesaran, D.J. Russel, J.W. Crawford, R. Rehn, E.A. Lewis, A unique calorimetric-cycler for evaluating high-power battery modules, in: Proceedings of the Long Beach Battery Conference, January, 1998.
[9] B. Culpin, J. Power Sources 133 (2004) 79.
[10] R. Wagner, J. Power Sources 53 (1995) 153.
[11] Z. Li, Y. Guo, L. Wu, M. Perren, H. Doering, J. Garche, J. Electrochem. Soc. 149 (2002) A934.
[12] D. Pavlov, J. Power Sources 64 (1997) 131.
[13] Pavlov, B. Monahov, J. Electrochem. Soc. 143 (1996) 3616.
[14] D. Pavlov, B. Monahov, J. Electrochem. Soc. 145 (1998) 70.
[15] D. Pavlov, A. Kirchev, B. Monahov, J. Power Sources 144 (2005) 521.
[16] R.S. Robinson, J.M. Tarascon, J. Power Sources 48 (1994) 277.
[17] R.K. Jaworski, J.M. Hawkins, Thermal runaway behavior of VRLA batteries, in: Proceedings of the Conference INTELEC'96, Boston, Massachusetts, October 6–10, 1996.
[18] F.J. Vaccaro, R.E. Landwehrle, Experiments on thermal runaway and its management for electrolyte immobilized lead-acid batteries, in: Proceedings of the Conference INTELEC'92, 1992, pp. 21–25.
[19] D. Brendt, E. Meissner, Proceedings of the Conference INTELEC'90, 1990, p. 148.
[20] S.D. Gerner, G.H. Brimyer, D.H. Bornemann, Proceedings of the Conference INTELEC'90, 1990, p. 161.
[21] A.I. Harrison, Proceedings of the Conference INTELEC'92, 1992, p. 28.
[22] S.S. Misra, T.N. Naveske, A.W. Williamson, Proceedings of the Conference INTELEC'92, 1992, p. 186.
[23] D. Pavlov, V. Naidenov, S. Ruevski, V. Mircheva, M. Cherneva, J. Power Sources 113 (2003) 209.
[24] P. Ruetschi, J. Power Sources 113 (2003) 363.
[25] D. Pavlov, S. Ruevski, V. Naidenov, G. Sheytanov, J. Power Sources 85 (2000) 164.
[26] G. Papazov, D. Pavlov, B. Monahov, J. Power Sources 113 (2003) 235.
[27] D. Pavlov, A. Kirchev, M. Stoycheva, B. Monahov, J. Power Sources 137 (2004) 288.
[28] D. Pavlov, I. Balkanov, T. Halachev, P. Rachev, J. Electrochem. Soc. 136 (1989) 3189.
[29] D. Pavlov, J. Electrochem. Soc. 139 (1992) 3075.
[30] S. Abaci, K. Pekmez, A. Yildiz, Electrochem. Commun. 7 (2005) 328.
[31] D. Pavlov, I. Balkanov, J. Electrochem. Soc. 139 (1992) 1830.
[32] P. Ruetschi, J. Ockerman, R. Amlie, J. Electrochem. Soc. 107 (1960) 325.
[33] B.N. Kabanov, E.S. Weisberg, I.L. Romanova, E.V. Krivolapova, Electrochim. Acta 9 (1964) 1197.
[34] J. Heyrowsky, Cas. Cesk. Lekarn 7 (1927) 242.
[35] A.I. Krasilshtikov, Zhurnal fisicheskoi khimii (Russ. J. Phys. Chem.) 21 (1947) 849.
[36] A.I. Krasilshtikov, Zhurnal fisicheskoi khimii (Russ. J. Phys. Chem.) 23 (1949) 332.
[37] Siver, B.N. Kabanov, Zhurnal fisicheskoi khimii (Russ. J. Phys. Chem.) 22 (1948) 53.
[38] I.M. Kolthoff, J. Jordan, J. Am. Chem. Soc. 74 (1952) 4801.
[39] S. Winkelmann, Z. Elektrochem. 60 (1956) 731.
[40] A.I. Krasilshtikov, B.A. Abdreeva, Zhurnal fisicheskoi khimii (Russ. J. Phys. Chem.) 27 (1953) 389.
[41] M.C. Davies, M. Clark, E. Yeger, F. Hovorka, J. Electrochem. Soc. 106 (1959) 56.
[42] W.B. Gu, C.Y. Wang, J. Electrochem. Soc. 147 (2000) 1910.